REPORT DOCUMENTATION PAGE

AFRL-SR-AR-TR-04-

0589

1. AGENCY USE ONLY *(Leave blank)*	2. REPORT DATE	3. REPORT TYPE AND DATES COVERED
		01 Sep 1999 - 31 May 2004 FINAL

4. TITLE AND SUBTITLE
(PECASE) Multiwavelength Optical Techniques for Communication and Computation

5. FUNDING NUMBERS
61103D
3484/SS

6. AUTHOR(S)
Dr Blumenthal

7. PERFORMING ORGANIZATION NAME(S) AND ADDRESS(ES)
UNIVERSITY OF CALIFORNIA
CHEADLE HALL
SANTA BARBARA CA 93106-2050

8. PERFORMING ORGANIZATION REPORT NUMBER

9. SPONSORING/MONITORING AGENCY NAME(S) AND ADDRESS(ES)
AFOSR/NE
4015 WILSON BLVD
SUITE 713
ARLINGTON VA 22203

10. SPONSORING/MONITORING AGENCY REPORT NUMBER
F49620-99-1-0324

11. SUPPLEMENTARY NOTES

12a. DISTRIBUTION AVAILABILITY STATEMENT
DISTRIBUTION STATEMENT A: Unlimited

12b. DISTRIBUTION CODE

20041129 029

13. ABSTRACT *(Maximum 200 words)*

In this research project the team studied unique gain and signal processing capabilities of semiconductor optical amplifiers (SOAs). The main areas studied over the 5 years of this award were: 1. Small signal processing using SOAs; 2. Large signal pulse shaping using SOAs; and 3. Optical signal processing and filtering using slow optical waveguides based on electromagnetically induced transparency (EIT). In this PECASE sponsored research they investigated the potential for compound semiconductor optical amplifiers (indium Phosphide) to serve as signal processing elements for various applications. Moving to the future, there is an opportunity to develop new materials and device structures that optimize the desired performance for small and large signal processing in SOAs. For large signal there is a need to develop InP amplifier structures that have ultrafast carrier recovery response time so that data rates out to 160Gbps and beyond can be supported. The field of EIT in compound semiconductors is so new, that this probably represents the biggest opportunity but is also the largest risk. Finding the correct compound semiconductor system that at room temperature can yield increases in refractive index by factors of 10, 100 and 1000 greater than possible today has the potential to shrink photonic circuits to nanometer dimensions as well as ultra high scale density integration.

14. SUBJECT TERMS

15. NUMBER OF PAGES

16. PRICE CODE

17. SECURITY CLASSIFICATION OF REPORT	18. SECURITY CLASSIFICATION OF THIS PAGE	19. SECURITY CLASSIFICATION OF ABSTRACT	20. LIMITATION OF ABSTRACT
Unclassified	Unclassified	Unclassified	UL

Final Technical Report for Presidential Early Career Award for Scientists and Engineers (PECASE) Program

F49620-99-1-0324 – Multi-Spectral Optical Techniques for Communication and Computation

October 30, 2004

Daniel J. Blumenthal
Department of Electrical and Computer Engineering
University of California, Santa Barbara, CA 93110
Tel: (805) 893-4169, Fax: (805) 893-5707, Email: danb@ece.ucsb.edu

Table of Contents

1 Executive Summary

In this research project we studied unique gain and signal processing capabilities of semiconductor optical amplifiers (SOAs). The main areas studied over the 5 years of this award were

1. Small signal processing using SOAs.
2. Large signal pulse shaping using SOAs.
3. Optical signal processing and filtering using slow optical waveguides based on electromagnetically induced transparency (EIT).

After summarizing the results of this research we discuss the potential future research directions.

2 Small Signal Processing using SOAs

In this work we investigated techniques to exploit the small-signal frequency response (SSFR) of a SOAs to process signals. In particular, we utilized a wavelength converter based on cross-gain modulation in a semiconductor optical amplifier with a finite waveguide loss. The result of this work was to correctly explain the signal processing (small signal) properties of SOAs where previous models did not. We developed a transfer function formalism to explain the resonant behavior of the frequency response. Operating with the data and CW signals in a co-propagating configuration, we find that the resonance only exists for a finite waveguide loss. In a counter-propagating scheme, a resonance can exist regardless of the presence of loss.

A theoretical analysis of the small-signal frequency response of a wavelength converter based on cross-gain modulation in a semiconductor optical amplifier with a finite waveguide loss was developed. We used this transfer function formalism to explain the resonant behavior of the frequency response. The limitations to the magnitude of the spectral overshoot are also accounted for. Operating with the data and CW signals in a co-propagating configuration, we found that the resonance only exists for a finite waveguide loss. In a counter-propagating scheme, a resonance can exist regardless of the presence of loss.

We consider an SOA in a XGM wavelength conversion scheme. This is shown in Figure 1, where $P_1(z)$ and $P_2(z)$ are the average powers of the data channel and CW channel at the position z respectively.

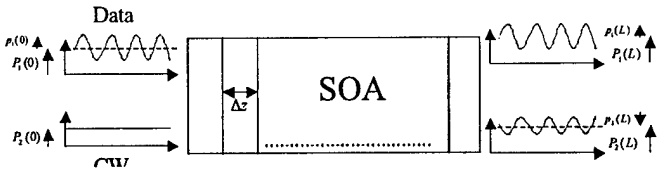

Figure 1. SOA traveling wave model structure.

The primary result of this work was an accurate accounting of the resonance peak that occurs in the RF transfer function and how loss plays a fundamental role in this behavior. Prior to this work there has not been an adequate traveling wave model description of how the resonance peak manifests and it dependence on loss. The previously developed formalism introduced in the previous section is used to explain why the RF transfer function of the CW channel may display a resonance when loss is introduced in the waveguide.

We define the spectral position $\Omega_{1/2}$ of a relative transfer function $H(z_n,\Omega)$ as the frequency at which it has reached the point halfway in between the low and high frequency limits. In all presented results, the following set of parameters are used: $P_T(0) = 3\text{mW}$, $P_{sat} = 10\text{mW}$, $\tau_s = 200\text{ps}$, $\gamma = 0.4$, $g_0 = 5\text{x}10^4\ \text{m}^{-1}$, and M=200. The magnitude of M does not change the total SSFR of the SOA. However, the characteristics of the

individual transfer functions will obviously change with M, since the product of all of them is independent of M. The amplifier length L is 1mm unless stated otherwise and the normalized loss ζ will be varied.

It is observed in Figure 2 that $\Omega_{1/2}$ is independent of ζ for $z = z_0$, which is anticipated since the loss has not yet had a chance to change the gain G at this early stage of the SOA. The contrast ratio $C_2(z)$ is observed to be independent of ζ in the rear of the SOA ($z=z_{N-1}$). Finally, it is clear that the transfer functions 'drift' less when loss is present, compared to the lossless case.

Fig. 3b shows $\Omega_{1/2}$ on a logarithmic scale as a function of τ_{eff} also on a logarithmic scale, for the same losses as in Figure 2a. Notice that the curve corresponding to $\zeta = 0$ is linear with a slope magnitude of 1, indicating that $\Omega_{1/2} = c\backslash \tau_{eff}^{-1}(z)$ for this case, where c is a constant. As ζ is increased, the curves deviate more and more from linearity, causing $\Omega_{1/2}$ to increase with ζ for a constant τ_{eff}. However, as illustrated in Figure 2a, a specific τ_{eff} is reached at a later stage in the amplifier when the loss is increased, due to the reduced change of τ_{eff} over the length of the SOA.

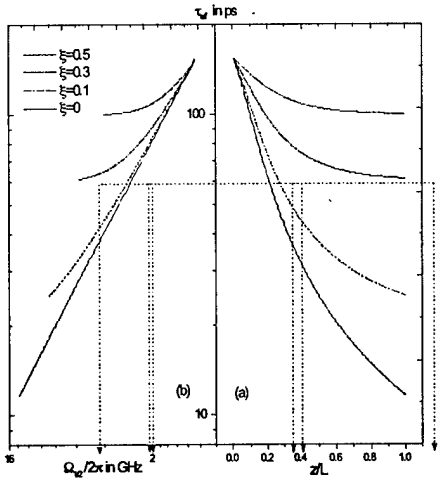

Figure 2. (a) The effective carrier lifetime vs. the normalized position inside the SOA for different values of the normalized loss. An increase of the loss causes an increase of the lifetime. (b) The spectral position vs. the effective carrier lifetime.

Figure 3 shows the evolution of $\Omega_{1/2}$ with z/L, and here it is clear that the 'drift' of the transfer functions is reduced significantly when ζ is increased. That means that in the cases where loss is present, the high-pass functions $H(z_n,\Omega)$ will tend to align themselves. When they are multiplied the alignment will cause the slope magnitude of the total high-pass function $\Pi_2(\Omega)$ to increase through resonant enhancement. The trend in Figure 3 is clear: the bigger the loss, the more effectively the transfer functions are aligned. However, the alignment will only establish itself as an overshoot if a value of Ω exists,

such that the logarithm of $|\Pi_2(\Omega)|$ has a larger slope magnitude than the logarithm of the low-pass function $|L(\Omega)|$.

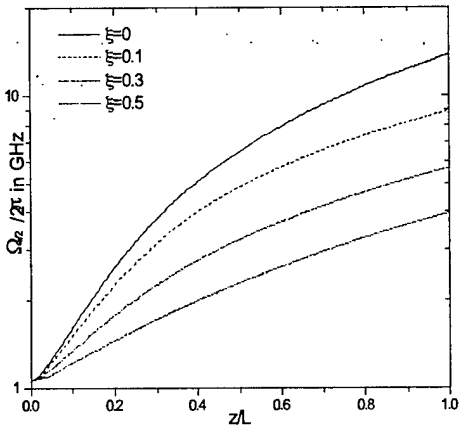

Figure 3. The spectral position of CW-transfer functions as a function of the normalized position for different normalized losses. An increase of the loss is seen to inhibit the 'drift' of the transfer functions.

Figure 4 shows the low-pass function $L(\Omega)$, and the total high-pass function $\Pi_2(\Omega)$ for $\zeta = 0$ and $\zeta = 0.5$, as well as the relative SSFR of the CW channel at the output of the SOA. The latter is the product of the two former, or in this logarithmic chart, the sum. It is clear from Figure 4 that the higher slope of $\log|\Pi_2(\Omega)|$ in the lossy case, results in an overshoot when the low-pass function is added.

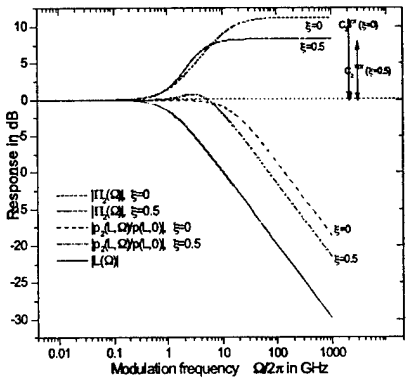

Figure 4. The low-pass characteristic $L(\Omega)$, the total high-pass function $|\Pi_2(\Omega)|$ and the total, relative response, equal to the product of the two former (or the sum in this logarithmic chart), as a function of the modulation frequency for $\zeta = 0$ and $\zeta = 0.5$.

Neglecting the loss dependence of the contrast ratio one would think that the magnitude of a possible overshoot would keep on increasing with ζ. However, the contrast ratio reveals a significant ζ-$dependence. This is shown in Figure 5, where $C_2(z_n)$ is seen to decrease as ζ is increased. This can be attributed to the reduction of the slope magnitude of $\tau_{eff}(z)$ in Figure 2a. The local maxima of the contrast ratio observed in Figure 5 are due to the fact that the τ_{eff} vs. z curves in Figure 2a have inflection points. The contrast ratio becomes independent of ζ towards the end of the amplifier. This is because the slopes of the curves in Figure 2a all approach the same value (zero) for z/L approaching 1.

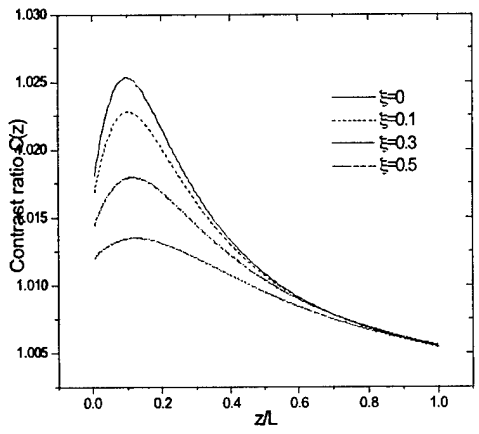

Figure 5. *The contrast ratio vs. the normalized position. Increasing the loss decreases the contrast ratio. The maxima are due to the existence of inflection points in Figure 2a.*

The contrast ratio of the total high-pass function is the product of the contrast ratios of all the individual relative transfer functions. From Figure 5 it is obvious that C_2^{TOT} must decrease with ζ and this is also clearly observed in Figure 4. This is the reason why the 3 dB modulation bandwidth decreases when loss is introduced. This is illustrated in Figure 6 (left), where the magnitude of the overshoot is shown as a function of the normalized loss for three different amplifier lengths. The unsaturated gain coefficient g_0 is kept constant, corresponding to a constant injection current density. For the set of parameters chosen, it is observed that for normalized losses up to ζ = 0.4-0.5, depending on the amplifier length, the alignment effect is dominant. At higher values of ζ the degradation of the contrast ratio takes over. Figure 6 (right) shows that for any given ζ there is a critical amplifier length L_{crit} below which no overshoot is observed. This effect has also been reported in the case where the bias current is modulated. For ζ approaching 0, L_{crit} goes to infinity, which is in agreement with the fact that no overshoot exists for loss-less waveguides operated in the co-propagating scheme. The critical length has a minimum around ζ = 0.4. It is important to stress that ζ can be manipulated by changing the bias current since ζ depends on g_0.

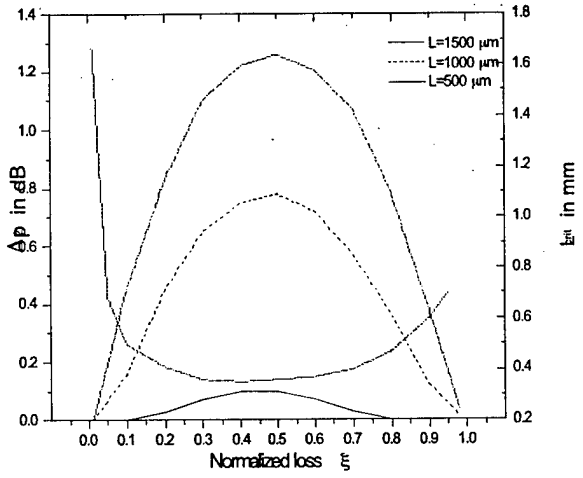

Figure 6. *The magnitude of the overshoot in dB for three different amplifier lengths (left) and the critical length, below which no overshoot is observed (right), vs. normalized loss.*

It follows from the above that the modulation bandwidth of the SOA increases when operated in the counter-propagating configuration. This is not true in reality, however, because of walk-off effects which cause a steep fall-off of the SSFR when the modulation frequency becomes comparable to the transit time of the SOA. However, the walk-off effects do not change the fact that the SSFR can display a resonance for zero waveguide loss. The predictions made above, based on the transfer function approach presented here, have been verified by an iterative small-signal model of the counter-propagation configuration.

2.1 Conclusion and Summary

In conclusion, in this part of the program, a transfer function approach to analyzing the small-signal frequency response of the CW channel in a XGM wavelength conversion scheme has been investigated. It was found that the existence of the RF resonance peak can be explained in terms of aligning high-pass transfer functions. The degradation of the response function that follows from the internal loss in the waveguide is also successfully explained from the transfer functions as a decrease of the contrast ratio. We find that no overshoot will be observed in the co-propagation scheme if the amplifier length is below a certain critical value. For the parameters used, we found that the critical length is minimum for the value $\zeta = 0.40$ of the normalized loss. Using the transfer function approach presented here, we conclude that a resonance of the SSFR can exist in the counter-propagating configuration, regardless of the presence of loss.

3 Large Signal Pulse Signal Processing using SOAs

The pulse extinction ratio (ER) in digital systems is a critical performance parameter. The ER, defined as the ratio between the peak pulse power and the maximum power of the unwanted background signal between the pulses, has to be very large to avoid interference between adjacent channels. In ultrafast optical systems, optical time division multiplexing (OTDM) is used to form high bit rate streams at rates greater than 40 Gbps. a practical transmitter, one pulse source is usually split into a number of channels and subsequently modulated with data. Due to the limited coherence time of the pulse source the phase of the optical carrier will change over time, and if the signal is interfering with another electric field, these phase changes are translated into amplitude fluctuations. In most published OTDM experiments a mode-locked fiber ring laser is used as a pulse source, which usually has a very good pulse ER (>40 dB). However, in practice it would be better if a cheap pulse source could be used, e.g. a $LiNbO_3$ modulator or an electroabsorption modulator (EAM). Unfortunately these pulse sources have a poor pulse ER, usually 15–25 dB, which limits their use in OTDM systems.

In this work we investigated the effects of a poor pulse ER on a 40 Gb/s OTDM system, and developed an SOA based technique to improve the pulse ER. A schematic of the technique is shown in Figure 7.

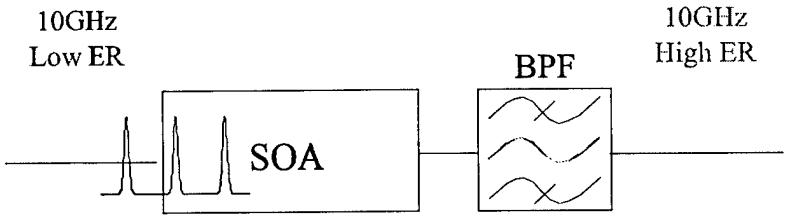

Figure 7. *Schematic diagram extinction ratio enhancement signal processing using an SOA.*

With sufficient input power to the SOA the pulse spectrum is broadened through saturation-induced SPM. The Broadening occurs mainly on the low-frequency (the red) side of the spectrum since the increase in phase caused by the stimulated recombination is much faster than the decrease due to gain recovery. The temporal variation of the frequency chirp approximately follows the output pulse shape, which means that the SOA translates pulse intensity into spectral shift. Consequently, filtering out the red-shifted part of the spectrum, the pulse ER can potentially be increased. Depending on the filtering, the spectral shift can also be accompanied by pulse compression, since the red-shifted peak is usually broader than the input spectrum.

Figure 8 a) shows an oscilloscope-trace of the 40Gb/s pulses without using the SOA to increase the pulse ER. The poor pulse quality is due to semi-coherent interference between the signal pulses and the very weak pulses introduced by the 'ER-degrader'. In Figure 8 c) the same trace is shown with the SOA inserted, and the improvement is apparent. The equivalent eye-diagrams are shown in Figure 8 b) and d).

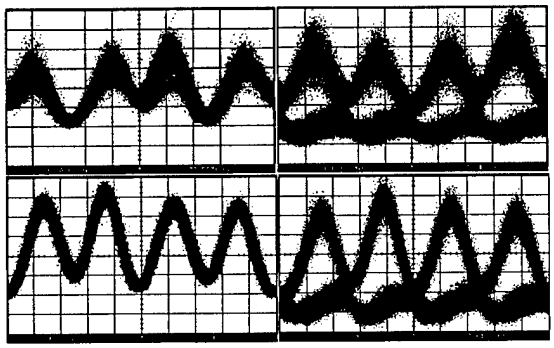

Figure 8. Top left (a): Trace of 40Gb/s pulse train w/o use of SOA. Top right (b): Corresponding eye-diagram. Bottom left (c): Trace of 40Gb/s pulse train w/ use of SOA. Bottom right (d): Corresponding eye-diagram.

The signal processing principal is shown in Figure 9 where the pulse is red shifted during the rising and falling edges of the input pulse.

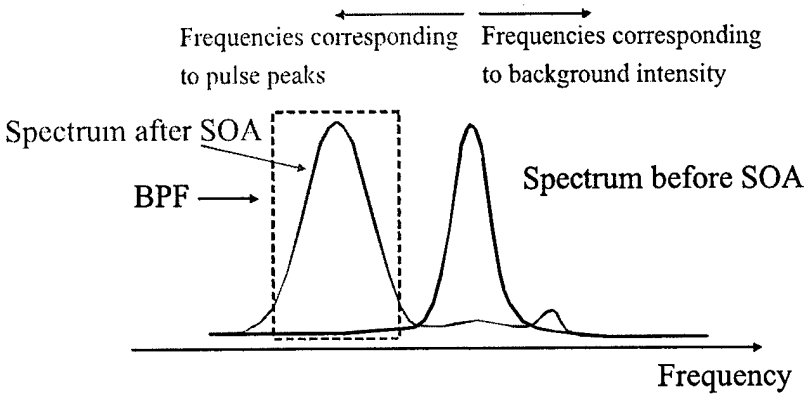

Figure 9. ER enhancement by following the intensity dependent frequency shift with an optical bandpass filter.

3.1 Conclusions and Summary

We have demonstrated that XPM in an SOA followed by a filter restores the pulse ER and removes the interference problems. Numerical investigations verify that the pulse ER can be improved from 20dB to >40dB by the technique used here. Problems with semi-coherent and incoherent interference are generally caused both by pulse overlap and by a finite pulse ER, but in this experiment the latter is the most dominant. This was verified by the fact that the system performance without the SOA did not improve by decreasing the input pulse width from 12ps to 8ps. This proves that the dramatic improvement obtained by using the SOA is not due to pulse compression.

4 Electromagnetically Induced Transparency

Electromagnetic induced transparency (EIT) is a nonlinear optical phenomenon that offers a possibility to dynamically engineer the susceptibilities of materials, potentially allowing for large increases in the density of photonic components, as well as the development of functions of impossible implementation with existing integrated optical technologies. EIT has been demonstrated in many different material systems, such as atomic gases, doped crystals and semiconductors.

EIT can be achieved in materials with three-level electronic systems as shown in Figure 10. Transparency for optical signals at the frequency of the a-b transition (signal field) is achieved through appropriate optical pumping at the a-c transition frequency (control field). It is a result of a coherent superposition of the eigenstates $|b\rangle$ and $|c\rangle$ in time, such that the system is trapped in a time-invariant state - the so-called ``dark state". This is possible, of course, if the degree of coherence between $|b\rangle$ and $|c\rangle$ in time is sufficiently high. Effectively, no a-b transitions occur in this case, in spite of the presence the signal field; the latter will, therefore experience no absorption. The same is valid for the control field.

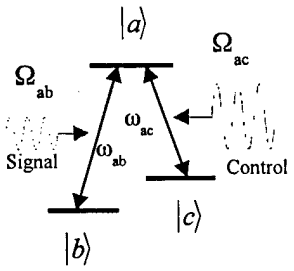

Figure 10. Three level system for describing EIT.

A direct application of using an EIT material with ultra large index of refraction is an ultra-compact optical filter. An example of a typical waveguide directional coupler filter is shown in Figure 11. The coupler consisting of two slab waveguides, 1 (input) and 2 (output), respectively with phase indices n_{1p} and n_{2p}, separated by a distance l and surrounded by a substrate material with phase index n_{sp}. Taken separately, guides 1 and 2 are designed to have only one guided mode each, with effective propagation constants β_1 and β_2, respectively, corresponding to mode effective indexes n_{1p} and n_{2p}.

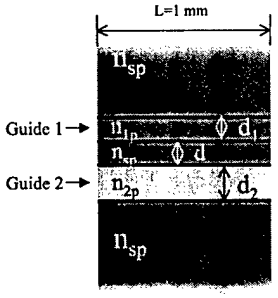

Figure 11. Waveguide directional coupler filter.

The bandwidth filter bandwidth for this expression can be obtained by looking at the variation of:

Eq.(4)
$$\Delta\lambda = \frac{\lambda_0^2}{L(N_{g1} - N_{g2})}$$

Where

$$N_{g1,2} = N_{p1,2} - \lambda \frac{dN_{p1,2}}{d\lambda}$$

are the group indexes of modes in waveguides 1 and 2, taken at the center frequency. It is apparent that the bandwidth could be made arbitrarily small by choosing guides with propagation constants that change with frequency (or wavelength) at sufficiently different rates around the operation frequency. The total dispersion in the waveguides has contributions both from the material and waveguiding mechanism, thus it can be tuned to very high values through optical pumping. In what follows, only the TE case was examined, but similar performance should be expected for TM waves. The following expression for group index was used in the calculations:

$$N_{ig} = \frac{\Gamma_i n_{ig} n_{ip} + (1+\Gamma) n_{sg} n_{sp}}{N_{ip}}; i = 1,2$$

where Γ_i is the confinement factor of the mode and n_{ig} is the group index due to material dispersion in guide *i*. For comparison, we take a typical design for a filter based on InGaAsP – based material, lattice-matched to InP. The following parameters are used:

- Center wavelength: $\lambda = 1.55$ μm
- Device length: $L = 1$ μm
- Substrate (InP) phase index: $n_{sp} = 3.166$
- Thickness of separation layer: $d = 1.66$ μm
- Guide 1:
  - Phase index: $n_{1p} = 3.54$
  - Thickness: $d_1 = 0.312$ μm
  - Material group index: n1g = 3.7198
- Guide 2:
  - Phase index: $n_{2p} = 3.44$
  - Thickness: $d_2 = 0.55$ μm
  - Material group index: n2g = 4.0831
- Guides 1 and 2 modal index: $N_{1p} = N_{2p} = 3.34$
- Filter bandwidth: $B = 11.503$ nm.
- Material group indices were obtained from [5] and [6].

A very narrow band, compact filter can be realized by replacing the material of guide 1 with a material capable of EIT (with the same refractive index when no control light is

applied). In the following results, an atom density Na = $1x10^{23}m^{-3}$ and dipole density $\wp_{ab}=1x10^{-9}$ were used. Both values are reasonable for semiconductor systems. A graph showing the coupler bandwidth as function of the Ω_{ab} Rabi frequency is shown in Figure 12.

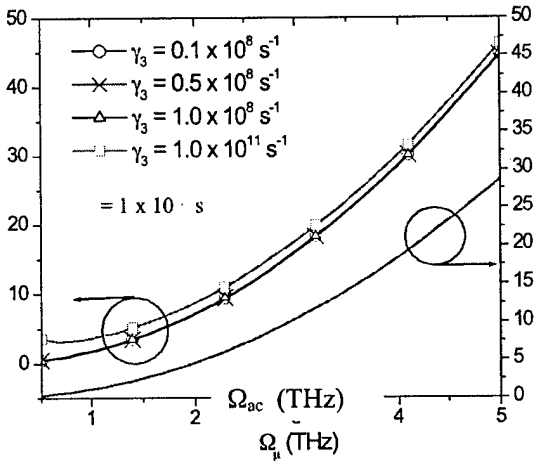

Figure 12. Coupler Bandwidth for EIT filter for fixed γ_1 and varying γ_3.

The power density estimate is as function of Ω_{ab} is also shown. The decoherence constant γ_1 was fixed at $\gamma_1 = 1 \times 10^{12}s^{-1}$ and γ_3 was varied. Very little change is observed in the coupler bandwidth for γ_3 varying between 1 MHz and 10 GHz, for the Rabi frequency range considered. Notice that the control signal power density as a function of Ω_{ac} is displayed in the figure as well, calculated from Eq. (4); it ranges approximately between 0.5 and 30 $mW/\mu m^2$. Sub-picometer bandwidths can be achieved at lower control signal powers. For γ_3 = 100 GHz , the bandwidth suffers a substantial increase at lower powers. At this point though, absorption at center frequency becomes rather high.

It is possible to define a transparency (or rather low-loss) window as the frequency range around the operation point where the overall losses for 1 mm length of the EIT waveguide are less than 3 dB. It is expected that such transparency window can accommodate several narrow-bandwidth channels at the same time.

As shown in figure 6, the coherence decay constant γ_3 has a very strong impact on the loss bandwidth, since it controls the attenuation at center frequency. In fact, for larger values, losses at the operation frequency become higher than 3 dB for low control power, thus the low-loss window cannot be defined, e.g. for γ_3 at 1, 0.5 and 0.1 GHz, the low-loss window ceases to exist at Ω_{ac} below 3.5, 2.5 and 1.0 THz respectively. Compared to the coupler bandwidth for γ_3 = 100 MHz, it would be possible to accommodate up to three channels within the transparency window, for a control power density of about 30 $mW/\mu m^2$.

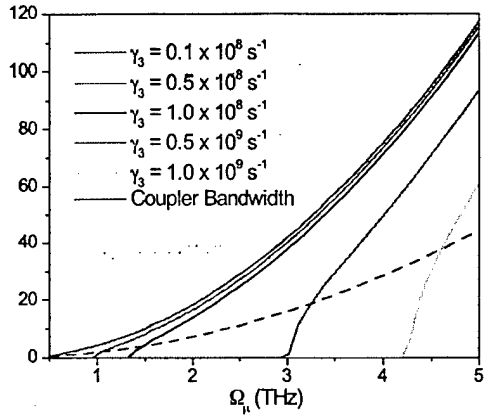

Figure 6: 3-dB loss bandwidth for various values of γ_3 and fixed γ_1.

The loss bandwidth could in principle be increased by decreasing the decoherence parameter between states a and b, γ_1. This parameter influences the linewidth of the system's resonances, thus it has an obvious influence on the achievable low-loss window. Figure 7 shows the change in the low-loss bandwidth for different values of γ_1 and γ_3 =100 MHz, within the same power density range. The coupler bandwidth is not significantly altered by this parameter as shown above, thus the same coupler bandwidth curve, shown as a dashed line in the picture can be used for comparison.

For γ_1 = 10 GHz, A rather large low-loss bandwidth of 1.2 nm can be achieved at 30 mW/μm^2 control power density, allowing for the accommodation of more than 20 40-picometer channels. It is clear from the above that very narrow-band, optically-controllable filtering characteristics can be achieved from an EIT coupler filter given some specific conditions. Mainly, one would wish to make the coherence times between the states as long as possible and also have a reasonably large control power density. The values of g1 and g3 used here are rather unrealistic when compared to what has been obtained experimentally so far in semiconductor systems. Also, some combinations of g1 and g3 will yield unrealistically large χ–values. Although such γ–values are found in atomic systems, in general the atom number density, N_a, as well as the dipole matrix element $\wp_{ab}$ are smaller than assumed here, leading to lower χ.

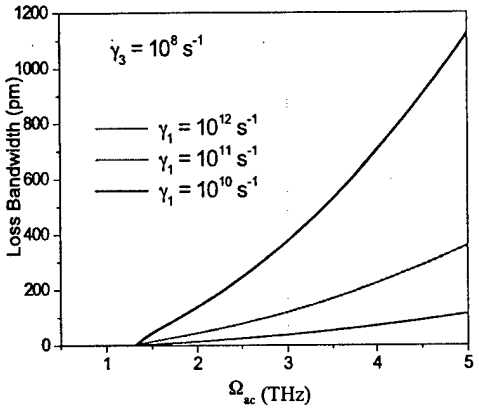

Figure 7: Loss Bandwidth for varying values of γ_1 and fixed γ_3.

4.1 Conclusions and Summary

It is clear from Section IV above that very narrow-band, optically-controllable filtering characteristics can be achieved from an EIT coupler filter given that coherence times can be made sufficiently long. The values of and used here, though, are rather unrealistic when compared to what has been obtained experimentally so far in semiconductor systems. A on the order of 100 GHz corresponds to the 1 ps dephasing time mentioned above, three orders of magnitude larger than values used in the previous calculations. The same calculations show that, for GHz and , the narrowest achievable coupler bandwidth is close to 3.5 nm, with a loss bandwidth of the same order of magnitude, for THz. This means that only one channel can be fit in the low-loss window. An improvement of one order of magnitude, on the other hand, yields a coupler bandwidth of 300 pm at THz, with enough loss bandwidth to accommodate four channels. Additionally, some combinations of and will yield unrealistically large values. Although such values are found in atomic systems, in general the atom number density , as well as the dipole matrix element , are smaller than assumed here, leading to lower . In conclusion, we have shown the possibility of using the huge dispersion inherent in EIT to generate narrowband filters, with bandwidths several orders of magnitude smaller for a given length than what has hitherto been reported with more conventional mechanisms for generating differential dispersion.

5 Prospects for Future Work

In this PECASE sponsored research we have investigated the potential for compound semiconductor optical amplifiers (indium Phosphide) to serve as signal processing elements for various applications. Moving to the future, there is an opportunity to develop new materials and device structures that optimize the desired performance fro small and large signal processing in SOAs. For large signal there is a need to develop InP amplifier structures that have ultrafast carrier recovery response time so that data rates out to 160Gbps and beyond can be supported. The field of EIT in compound semiconductors is so new, that this probably represents the biggest opportunity but is also the largest risk. Finding the correct compound semiconductor system that at room

temperature can yield increases in refractive index by factors of 10, 100 and 1000 greater than possible today has the potential to shrink photonic circuits to nanometer dimensions as well as ultra high scale density integration.

6 Personnel Supported

- Marcelo Davanco (Ph.D Student)
- Wenbin Zhao (PhD Student)
- Roopesh Doshi
- Mads Neilson
- Tommy Berg

7 Publications

/1/ "An extremely narrowband directional coupler wavelength filter based on electromagnetically induced transparency," Marcelo Davanço, Daniel Blumenthal, Lars Thylén, in OSA *Trends in Optics and Photonics (TOPS) Vol. 78, Integrated Photonics Research,* OSA Technical Digest, Post Conference Edition (Optical Society of America, Washington DC, 2001), pp. IThF2-1-3

/2/ "Directional Coupler Wavelength Filters Based on Waveguides Exhibiting Electromagnetically Induced Transparency," M. Davanco, P. Holmstrom, D. J. Blumenthal, L. Thylén, *IEEE Journal of Quantum Electronics,* 39 (4), pp. 608-13, April (2003).

/3/ "A Transfer Function Approach to the Small-Signal Response of Saturated Semiconductor Optical Amplifiers," M. Nielsen, D. J Blumenthal, and J. Moerk, IEEE Journal of Lightwave Technology, 18(12), pp. 2151-2157, December 2000.

/4/ "Pulse Extinction Ratio Improvement Using SPM in an SOA for OTDM Systems Applications," M. L. Nielsen, B. E. Olsson, and D. J. Blumenthal, IEEE Photonic Technology Letters, 14(2), pp. 245-247, February 2002.

/5/ "Pulse Extinction Ratio Improvement Using SPM in an SOA for OTDM systems applications," M. L. Nielsen, B. E. Olsson, D. J. Blumenthal, Proceedings of the 26th European Conference on Optical Communication (ECOC 00), Munich, Germany, Paper 1.1.6, pp. 23-24, September 4-7, 2000.